

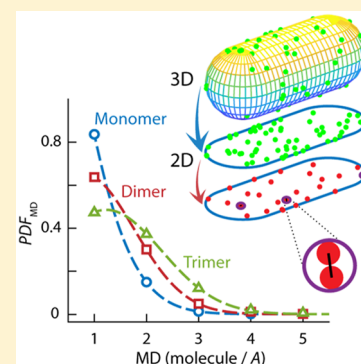
Quantifying the Oligomeric States of Membrane Proteins in Cells through Super-Resolution Localizations

Xihong Xie,[†] Yu-Shan Cheng,[†] Meng-Hsuan Wen, Aparna Calindi, Karen Yang, Chi-Wei Chiu, and Tai-Yen Chen^{*@}

Department of Chemistry, University of Houston, Houston, Texas 77204, United States

Supporting Information

ABSTRACT: Transitions between different oligomeric states of membrane proteins are essential for proper cellular functions. However, the quantification of their oligomeric states in cells is technically challenging. Here we developed a new method to quantify oligomeric state(s) of highly expressed membrane proteins using the probability density function of molecule density (PDF_{MD}) calculated from super-resolution localizations. We provided the theoretical model of PDF_{MD} , discussed the effects of protein concentration, cell geometry, and photophysics of fluorescent proteins on PDF_{MD} , and provided experimental criteria for proper quantification of oligomeric states. This method was further validated using simulated single-molecule fluorescent movies and applied to two membrane proteins, UhpT and SbmA in *E. coli*. The study shows that PDF_{MD} is useful in quantifying oligomeric states of membrane proteins in cells that can help in understanding cellular tasks. Potential applications to proteins with higher oligomeric states under high concentration and limitations of our methodology were also discussed.



1. INTRODUCTION

Transitions between different oligomeric states of membrane proteins are essential in the regulation of apoptosis,¹ tumor formation,² and signal transduction.³ However, to experimentally determine oligomeric states of membrane proteins is not trivial, especially when different oligomeric states coexist. Multiple methods have been applied to identify the oligomeric states of membrane proteins. Ensemble-based methods including chemical cross-linking,⁴ Förster resonance energy transfer,⁵ fluorescence cross-correlation spectroscopy,⁶ and number and brightness analysis⁷ are well-suited to measure the substantial fractions of oligomer but lack the sensitivity to quantify the subpopulation distributions if proteins exist in multiple oligomeric states.

Single-molecule localization microscopy (SMLM)-based approaches have also been applied to quantify oligomeric states of membrane proteins.^{8–12} The SMLM-based methods typically involve protein labeling and probe the oligomeric state by stochastic bleaching, blinking behaviors of organic fluorophores or fluorescent proteins (FPs), pair correlation analysis, or protein colocalization within the region of interest.^{13–17} For example, Durisic et al., Ulbrich et al., and Fricke et al. extracted the oligomeric state of membrane proteins in cells by counting either the photobleaching steps or the number of blinking events of FPs within an area of interest.^{13–15} Kasai et al. examined the monomer–dimer dynamic equilibrium using the colocalizations of labeled GPCRs via single-molecule tracking.^{16,18} The number of bleaching steps and blinking events are directly related to the numbers of FPs and will change under different protein concentrations. These methods are especially useful for cells

with low protein concentrations where the interference of neighbor proteins is minimized. However, for proteins abundantly present in the cells, quantification of their oligomeric state is still lacking. Given that cells often use concentration as a way to regulate cellular properties,^{9,19–22} it is essential and necessary to determine the oligomeric state of membrane proteins under high protein concentrations. A quantification method effectively removing the complication of protein concentration is especially useful for research involving prokaryotic cells, which typically are only μm in size and because the concentration effect cannot be ignored with prokaryotic cells. Veatch et al. used correlation functions to quantify clustering in super-resolution fluorescence localization images, and they included the protein concentration variables for the first time in their analysis.¹⁷ However, systematic analysis of the correlation between protein oligomeric state and protein concentration is still lacking.

Here we report a new single-molecule method to detect the oligomeric states of membrane proteins in *E. coli* and discuss how intracellular protein concentration affects the quantification through super-resolution localizations. First, using a theoretical model, we showed that the oligomeric states and the fraction of different oligomeric species for membrane proteins could be determined by the probability density function of molecule density (PDF_{MD}). We then discussed the effects of protein concentration, cell geometry, and photophysics of fluorescent proteins for the analysis as well as

Received: October 25, 2018

Revised: October 31, 2018

Published: November 1, 2018

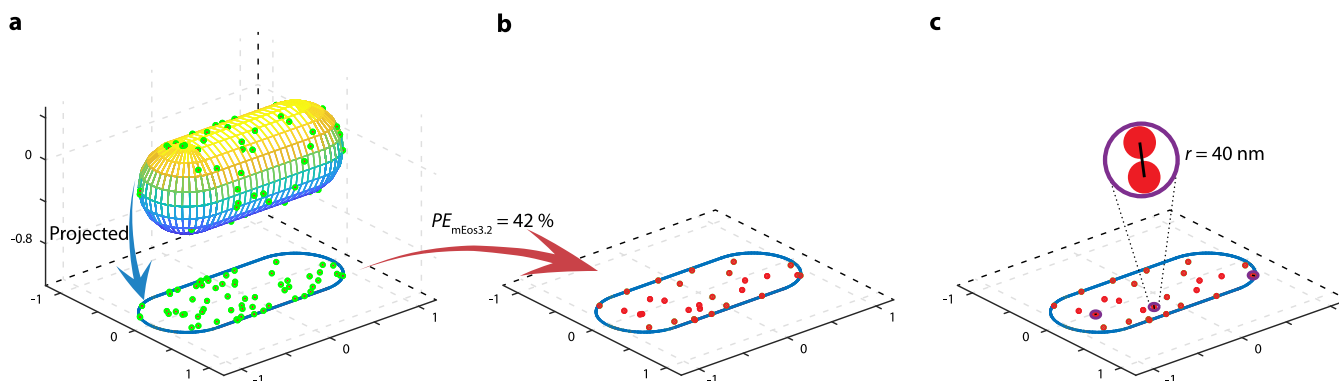


Figure 1. Single-molecule imaging data simulation. (a) Locations of membrane proteins were first generated in the 3D cell model. Projecting 3D data onto the xy plane generated the 2D simulated data. (b) A subset of the 2D locations of membrane proteins was randomly sampled to reflect photoconversion efficiency of mEos3.2 ($PE_{\text{mEos3.2}} = 42\%$). (c) Calculation of the pairwise distance between molecules. Molecules within the $r = 40$ nm circular area were grouped to estimate the molecule density.

provided experimental criteria for proper quantification of oligomeric states. After validating this method using simulated SMLM movies, we further demonstrated a successful application to the experimental SMLM data of a monomeric sugar phosphate antiporter, UhpT, and a peptide antibiotic transporter, SbmA, in *E. coli*. Potential applications to proteins with higher oligomeric states under high concentration and limitations of our methodology were also discussed using theoretical models.

2. METHODS

2.1. Simulations of the Spatial Distribution of Membrane Proteins in Confined Space. Monomeric molecules of membrane proteins were randomly placed on the cell surface to mimic protein locations observed in single-molecule fluorescent images. We first modeled the three-dimensional (3D) cell geometry as a cylinder capped by two hemispheres²³ for simplicity with cell length and width adapted from our experimental results. Within a single cell, a set of x , y , and z coordinates (i.e., one location) were randomly generated and only accepted when points were intersecting with the cell surface. This procedure was repeated until achieving a total molecule number (N_t) of 300 to 4800. Results were the averages of the simulations from 900 cells to ensure statistically saturated conclusions.

For the spatial distribution of multimeric membrane proteins (i.e., dimer, trimer, tetramer, pentamer, and hexamer), locations of molecules other than the initial location are simulated using a two-dimensional (2D) Brownian diffusion model. In short, with a chromosome diffusion^{19,24} constant $D = 0.025 \text{ mm}^2\text{s}^{-1}$ and a time resolution $t = 0.04 \text{ ms}$, we generated the distribution of displacement vector (\vec{r}_i , where $i = x$ or y) following $P(\vec{r}_i, t) = \frac{1}{4\pi Dt} \exp\left(-\frac{r^2}{4Dt}\right)$. We randomly chose an \vec{r}_i from the distribution of the displacement vector to perform the 2D diffusion on a 3D curved surface and calculate the subsequent positions. These new positions, together with the initial position, then constituted the random orientations of each molecule within the multimeric proteins with an average size of 2 nm. This step was repeated until all the locations of molecules were determined. Finally, the corresponding 2D simulated data were generated from 3D data by discarding the location information in the z -direction (Figure 1a, bottom). Note that all simulations will contain the same number of

molecules (N_t) rather than the same number of protein complexes. For example, a trimeric membrane protein will only have one-third of initial locations compared to that of the monomeric protein. The final location list of membrane proteins was created by randomly sampling a subset of this location list to reflect the finite photoconversion efficiency ($PE_{\text{mEos3.2}} = 42\%$, Figure 1b)^{13,25} of mEos3.2.

2.2. Generation of PDF_{MD} for Membrane Protein with Single Oligomeric State. With the simulated locations, the pairwise distances between molecules were calculated (Figure 1c). Molecules close to each other were grouped into the same cluster based on their pairwise distances. For the single-molecule super-resolution imaging condition, the minimum required distance to distinguish two adjacent objects is typically 4 times the localization precision.²⁶ Considering our localization precision of 20 nm, molecules with a pairwise distance shorter than 80 nm were first grouped into the same cluster. If assigned into multiple clusters in the first place, the molecule will be regrouped into the cluster where the distance between the molecule and the center-of-mass of the cluster is the shortest. This process generated a distribution of molecule density (i.e., MD, number of molecules within each circular area A , $A = \pi r^2$, $r = 40 \text{ nm}$), which is then normalized to the area to create the probability density function of molecule density (PDF_{MD} , Figure 2a).

2.3. Generation of PDF_{MD} of Membrane Proteins with Multiple Oligomeric States. The corresponding simulation of membrane proteins existing in multiple oligomeric states was generated through two steps: First, various fractions of 2D data were mixed while maintaining the same total number of molecules. Second, the mixed locations were sampled based on the photoconversion efficiency of mEos3.2. For example, we assumed the dimeric membrane protein exists as dimer and monomer with a fractional population of 60 and 40%, respectively. We sampled 30% dimeric proteins (two molecules per dimeric protein) and 40% monomeric proteins from the original dimeric and monomeric pools so that the total number of molecule remained the same after mixing. These locations were further selected according to the $PE_{\text{mEos3.2}}$ to result in the final locations for subsequent clustering. Locations within 40 nm radius were grouped to produce the PDF_{MD} as described in section 2.2.

2.4. Simulation of Single-Molecule Imaging Data with Photophysics of mEos3.2 Integrated. To mimic the experimental single-molecule imaging condition using

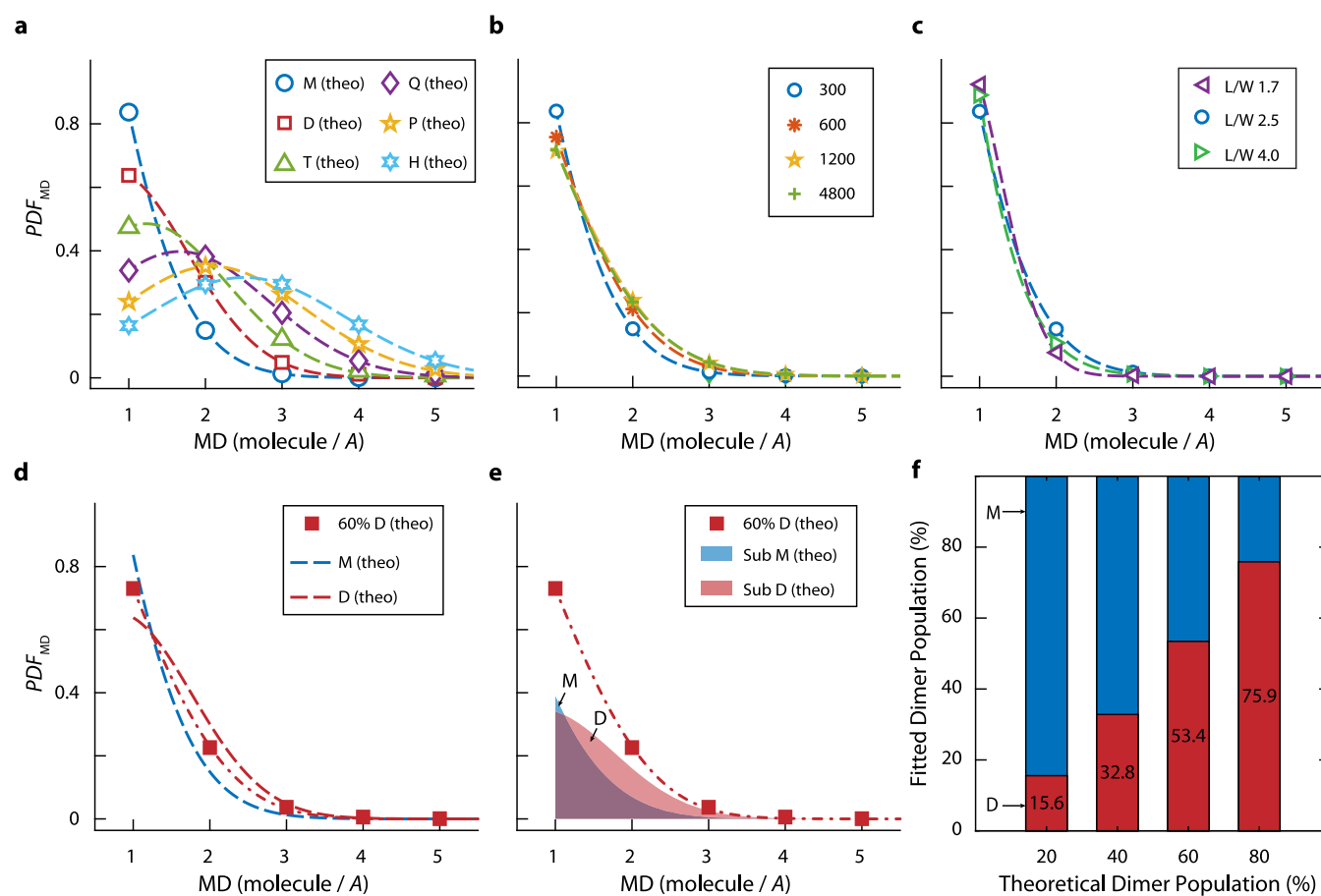


Figure 2. PDF_{MD} estimated from protein locations based on the theoretical model. (a) PDF_{MD} of membrane proteins with different oligomeric states under N_i of 300. Dash lines represent the corresponding truncated Gaussian fitting results. The different PDF_{MD} distributions of monomer (M), dimer (D), trimer (T), tetramer (Q), pentamer (P), and hexamer (H) suggest that the PDF_{MD} method is effective to differentiate membrane proteins with the oligomeric state varying from monomer to hexamer. (b) N_i and (c) cellular geometry-dependent PDF_{MD} of monomeric membrane proteins. L and W denote the length and width of a cell. (d) PDF_{MD} of the dimeric membrane protein with 40:60 (M/D) subpopulations (solid square) and its fitting result (dash-dot line) fall in between the PDF_{MD} of the pure monomeric (blue dash line) state and that of the dimeric (red dash line) state. (e) Fitting the PDF_{MD} in d with a combined truncated Gaussian function resolved the subpopulations of monomer (blue shade) and dimer (red shade). (f) Fitting results of relative populations of membrane dimeric protein existing in the various monomer to dimer subpopulations. Error bars for all simulated PDF_{MD} are within $\sim 5\%$.

mEos3.2, we generated the corresponding single-molecule fluorescent movies by modeling the photon conversion and photophysics of mEos3.2 within an appropriate cell shape by MATLAB. This approach approximated the detection of fluorescently tagged proteins in *E. coli* cells. The algorithm of our simulation method included the following procedures: (1) building a sequence of photoconversion events of the membrane proteins, (2) implanting the photophysics of mEos3.2, and (3) rendering each location with a point-spread function (PSF) and noise. In short, after the generation of random localizations on the cell membrane, we selected 42% of the localizations to reflect the photoconversion efficiency of mEos3.2. Each of these chosen localizations undergoes a series of blinking and bleaching events to reflect the photophysics of mEos3.2 and generates the localization sequences. Simulated locations in each sequence were convoluted with a PSF with a full width at half-maximum of 300 nm. Finally, the background noises were added to all PSFs so that the averaged signal-to-noise ratio of each image is comparable to our experimental conditions and produces the simulated single-molecule fluorescence images and movie.

2.5. Sample Preparation and Super-Resolution Imaging. Single-molecule fluorescent movies were collected through a similar approach as reported by Chen et al. (see details in the SI, sections 2 and 3).^{19,23} Briefly, we fused membrane proteins UhpT and SbmA with mEos3.2 by molecular cloning and expressed them in BW25113 and JW0358-1 *E. coli* strains, respectively. We then performed photoactivated localization microscopy (PALM) to localize the 2D locations of individual fusion proteins UhpT-mEos3.2 and SbmA-mEos3.2 in fixed *E. coli* cells at a sampling rate of 33.3 Hz under 561 nm laser power density of 6.5 kW/cm² (i.e., k_b of 35 ± 5 s⁻¹) until the mEos3.2 tag was photobleached (SI, section 5).

3. RESULTS AND DISCUSSION

3.1. Theoretical PDF_{MD} of Membrane Proteins with Different Oligomeric States. Figure 2a shows the PDF_{MD} of membrane proteins with oligomeric states ranging from monomer (M) to hexamer (H) under an N_i of 300. The PDF_{MD} of membrane proteins with different oligomeric states shows unique distributions, and the peak of the PDF_{MD} shifts to higher MD when moving from monomer (M) to hexamer

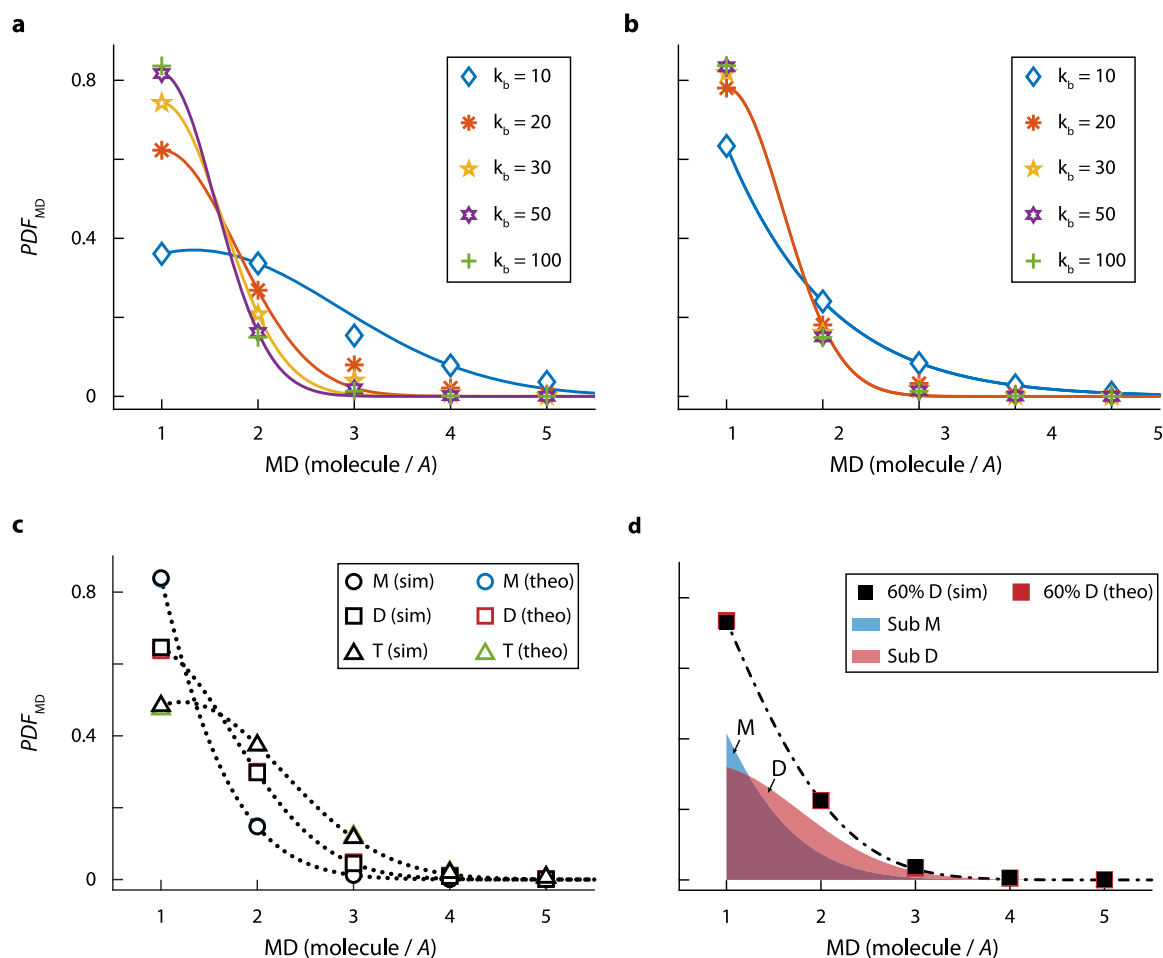


Figure 3. PDF_{MD} estimated from protein locations extracted from simulated images. (a) Photobleaching effect on PDF_{MD} of monomeric membrane protein at different photobleaching rate constants, k_b . (b) Same as a but after removing duplicated localizations. (c) Oligomeric-state-dependent PDF_{MD} estimated from simulated images agrees well with the theoretical model. (d) PDF_{MD} estimated from simulated images (black solid square) is consistent with the theoretical values (red solid square). The fitting result (dash-dot line) represents the sum of monomeric (blue shade) and dimeric (red shade) subpopulations.

(H), suggesting that PDF_{MD} can differentiate membrane proteins with different oligomeric states.

Since PDF_{MD} is directly related to the total number of molecules inside the cells, we evaluated the effect of molecule concentration on PDF_{MD} in differentiating the oligomeric states. Figure 2b shows the PDF_{MD} of monomeric membrane proteins with N_t varying from 300 to 4800. The PDF_{MD} shows a broadened distribution as the N_t increases and reaches a steady state when $N_t > 1200$. This deviation is because of the shortened distances between molecules under high molecule concentration. Such a condition resulted in grouping molecules from neighboring proteins and changed the PDF_{MD} . On the other hand, the low molecule concentration conditions naturally eliminate the potential incorrect grouping but will require averaging more cells to reach the statistically saturated conclusion. On the basis of our simulation, it will need averaging over 200 cells for membrane proteins with lower oligomeric states (i.e., monomer to trimer) under low molecule concentration conditions to achieve stable results (SI, Section 4). As for membrane proteins with higher oligomeric states (i.e., tetramer and above), averaging over 200 cells with a high concentration (~ 1000 locations) is needed. In addition to molecule concentration, cellular geometry can also affect the PDF_{MD} . Figure 2c shows the PDF_{MD} for cells with aspect ratios

(i.e., cell length/cell width) of 1.7, 2.5, and 4, which represent the cells with typical, doubled width, and doubled length cellular geometries, respectively. The increase in length or width will both increase the cellular volume and thus shift the PDF_{MD} toward to the low MD.

The PDF_{MD} of monomeric to hexameric conditions can be well-described by a truncated Gaussian function (Figure 2a), where the fitted centers and widths both provide information on the oligomeric state of membrane proteins (details in section 3.4). The center locations of the fitting results move to a higher MD for higher oligomeric states as expected. More importantly, our theoretical model also works for membrane proteins existing in mixed oligomeric states.

For example, Figure 2d shows the simulated PDF_{MD} of the membrane protein with monomer and dimer coexisting in a ratio of 40:60. The PDF_{MD} falls between the PDF_{MD} of pure monomeric and dimeric states. We determined the subpopulation of a target protein by fitting the PDF_{MD} with a combined truncated Gaussian function $f = p_d G_d + (1 - p_d) G_m$, where G_d and G_m are the theoretical truncated Gaussian functions for pure dimer and monomer, respectively. p_d and $(1 - p_d)$ represent the fractions of the dimeric and monomeric states, respectively (Figure 2e). The same analysis was performed across various subpopulation conditions. The

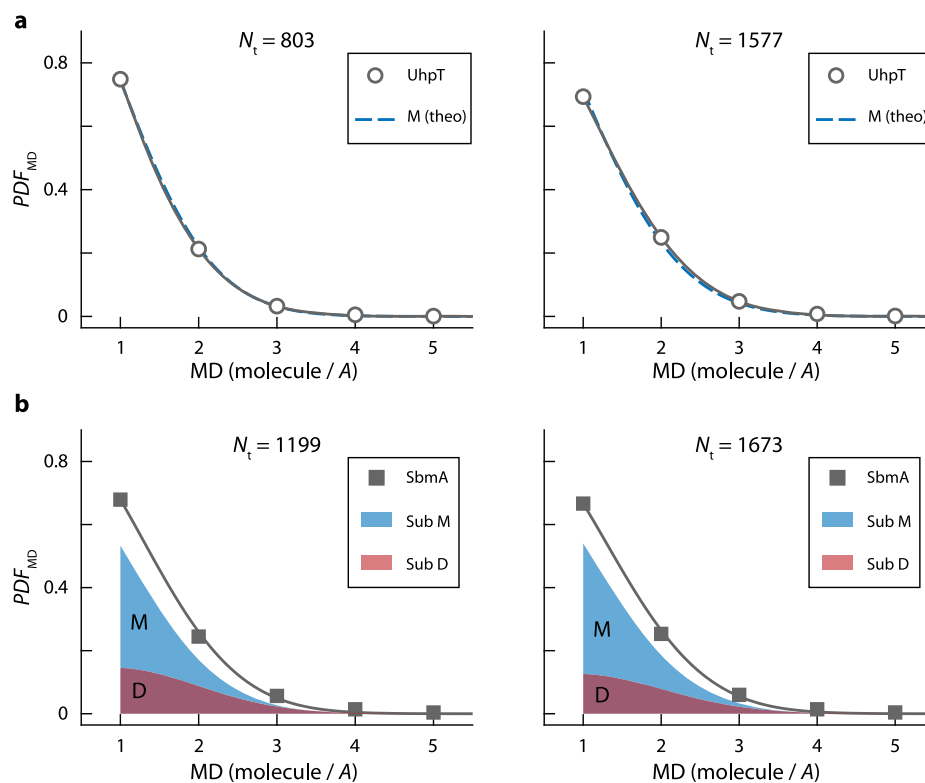


Figure 4. PDF_{MD} estimated from experimental data of UhpT and SbmA. (a) Comparison between the experimentally determined PDF_{MD} of UhpT and theoretical PDF_{MD} of the monomeric protein under different N_t . (b) Same as a but for SbmA.

comparison between theoretical and fitted subpopulations was summarized in Figure 2f, where the averaged errors (the difference between theoretical and fitted values over the theoretical value) of all four conditions are within 15%. Together, these results demonstrate that PDF_{MD} can effectively differentiate membrane proteins with different oligomeric states and determine the relative populations of proteins existing in multiple oligomeric states.

3.2. Validation of Theoretical PDF_{MD} with Simulated Single-Molecule Image Data. We verified our theoretical model using simulated single-molecule fluorescence images with the photophysics of mEos3.2 implanted. To mimic the experimental single-molecule imaging condition using mEos3.2, we generated the corresponding movies of single-molecule fluorescence images by modeling the photoconversion and photophysics of mEos3.2 within an appropriate cell geometry with the two-state model²⁷ using MATLAB (SI, section 5). The simulated images faithfully reproduced the photophysics of mEos3.2 and therefore were suitable to validate the feasibility of PDF_{MD} in quantifying the oligomeric states of membrane proteins.

The simulated images are then analyzed by the home-built MATLAB program iqPALM¹⁹ to extract the locations of individual molecules. The laser-excitation-intensity-dependent PDF_{MD} of monomer protein (Figure 3a) shows that the blinking events broaden the PDF_{MD} and shift the peak to the higher MD under low excitation density (i.e., the slow photobleaching rate, k_b). This problem gets even worse for membrane proteins with the higher oligomeric state because of higher probability grouping the blinking events within a cluster. The high laser power excitation can typically reduce this complication because of blinking events. Once the power density is high enough to result in a $k_b > 50 \text{ s}^{-1}$, the PDF_{MD}

then merges within 5% error. However, for research where phototoxicity is a concern and high laser power density is not preferred, proper estimation of PDF_{MD} can be achieved by implanting an algorithm to remove repeated localizations. In the algorithm, the interdistances of locations in adjacent frames were first calculated. If the distance is smaller than 2 times the localization precision, localizations in the later frames were considered as the same spot and thus removed. The remaining localizations then constitute the final PDF_{MD} . Figure 3b demonstrates that, after removing duplicated localizations, the PDF_{MD} merged under a much lower photobleaching rate ($k_b > 20 \text{ s}^{-1}$).

Simulated monomeric, dimeric, and trimeric single-molecule images with k_b of 100 s^{-1} are used to generate the corresponding PDF_{MD} for validating our quantification method. Molecule locations and repeated locations in the adjacent frame were extracted and removed respectively as described previously. PDF_{MD} resulting from fitted locations of purely monomeric, dimeric, and trimeric conditions agree excellently with the theoretical values (Figure 3c). The oligomeric-state-dependent PDF_{MD} retains the same trend regardless of the choice of r (SI, Section 5.2). Furthermore, for PDF_{MD} resulting from dimeric proteins with mixed monomeric and dimeric populations, fitting PDF_{MD} with the combined truncated Gaussian function recovers the individual population within 10% error (Figure 3d). These results collectively validated that PDF_{MD} is useful in quantifying oligomeric states of membrane proteins.

3.3. Determination of Oligomeric States of Highly Expressed Membrane Proteins with PDF_{MD} . After confirming that PDF_{MD} is effective to probe the oligomeric states of membrane proteins by using simulated single-molecule fluorescent movies, we applied this method to two

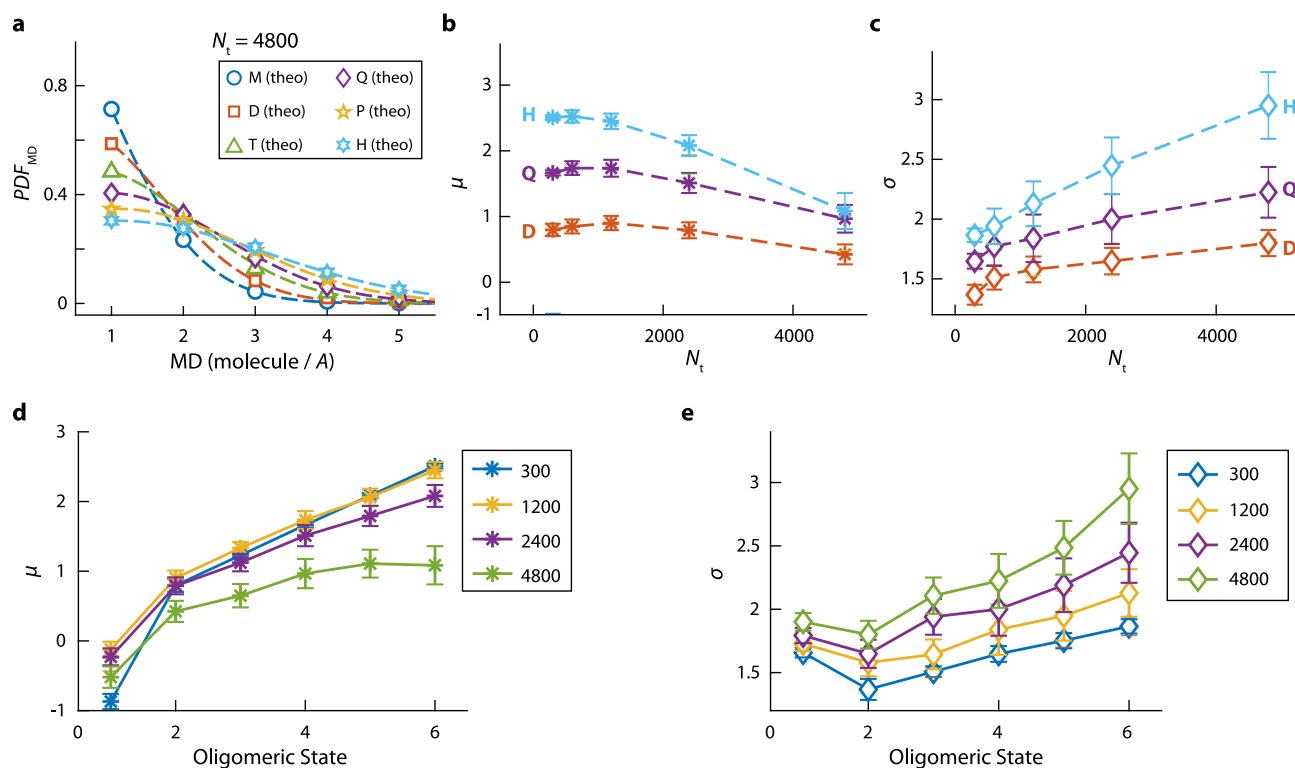


Figure 5. (a) PDF_{MD} of membrane proteins with different oligomeric states under N_t of 4800. (b,c) Mean (μ) (b) and width (σ) (c) of fitted PDF_{MD} as a function of N_t for dimer (D), tetramer (Q), and hexamer (H). (d,e) Oligomeric-state-dependent μ (d) and σ (e) under various N_t of 300, 1200, 2400, and 4800.

membrane proteins, UhpT and SbmA, in *E. coli* cells to extract their oligomeric states.

To compare the experimental data and our theoretical model directly, we minimized the effect of protein concentration and cell geometry by only selecting cells with similar sizes and molecule concentrations. Note that the single-molecule super-resolution imaging allows simultaneous quantifications of localizations of each membrane protein molecule and the overall molecule concentrations for each cell. This unique advantage enables the deconvolution of protein concentration from the determination of oligomeric states of membrane proteins. Overcounting due to photophysics of mEos3.2 were alleviated by removing repeated spots in the subsequent frames and imaging cells with a high laser power density of 6.5 kW/cm^2 (i.e., $k_b = 35 \text{ s}^{-1}$).

Membrane protein UhpT is a transporter protein that facilitates the uptake of phosphorylated hexose molecules into *E. coli* and has been reported presenting as a monomer through size-exclusion chromatography.²⁸ Figure 4a shows the comparison between the experimentally determined PDF_{MD} of UhpT and the corresponding monomeric simulation under two high molecule concentrations. Note that at each concentration, the theoretical model is generated based on the experimentally determined molecule concentration and cell geometry. The experimental determined PDF_{MD} of UhpT shifts toward the higher MD region with an increasing number of molecules. More importantly, the simulated PDF_{MD} describes the experimental data well at both protein concentrations (<5% error). It not only suggests that UhpT is indeed existing as a monomer in the cell but also validates that PDF_{MD} is effective in quantifying the oligomeric states of membrane proteins in cells.

We then performed the same analysis on the dimeric membrane protein, SbmA. SbmA is a transporter protein involved in the uptake of diverse substrates such as microcin B17 and J25, bleomycin, and peptide nucleic acid.^{29,30} Runti et al.²⁹ have reported that SbmA functions as a dimer but can also exist as a monomer through bacterial two-hybrid and cross-linking assays. Figure 4b shows the experimentally determined PDF_{MD} of SbmA under two molecule concentrations. The PDF_{MD} falls in between the simulations of pure monomeric and dimeric states. This discrepancy clearly indicates that SbmA exists in more than one oligomeric state.

To dissect the relative subpopulations in different oligomeric states, we tentatively fitted the PDF_{MD} of SbmA with a combined truncated Gaussian model (assuming SbmA has both monomeric and dimeric states) as described previously. The fitting results quantified $\sim 30\%$ of SbmA existing as the dimer and 70% as the monomer.

If considering SbmA as a self-associating dimerizing protein, the equilibrium of the self-associating dimerizing proteins can

be described as $M + M \xrightleftharpoons{K_D} D$, where M, D, and K_D represent the monomer, dimer, and equilibrium dissociation constant, respectively. K_D can be expressed in terms of the concentrations of M ($[M]$) and D ($[D]$) through $K_D = [M]^2/[D]$. The concentration of total monomers ($[M]_T$) can be expressed as $[M]_T = [M] + 2[D]$. This will give $[D] = ([M]_T - [M])/2$. Substituting the $[D]$ in the K_D equation with the $[D]$ expressed in terms of $[M]$ and $[M]_T$ results in $K_D = 2[M]^2/[M]_T - [M]$. Localizations of each molecule were determined by fitting individual point-spread functions with a 2D Gaussian function. After the photoconversion efficiency was corrected, number of moles of protein can be estimated via dividing the number of molecules by the Avogadro constant. Dimensions of each cell

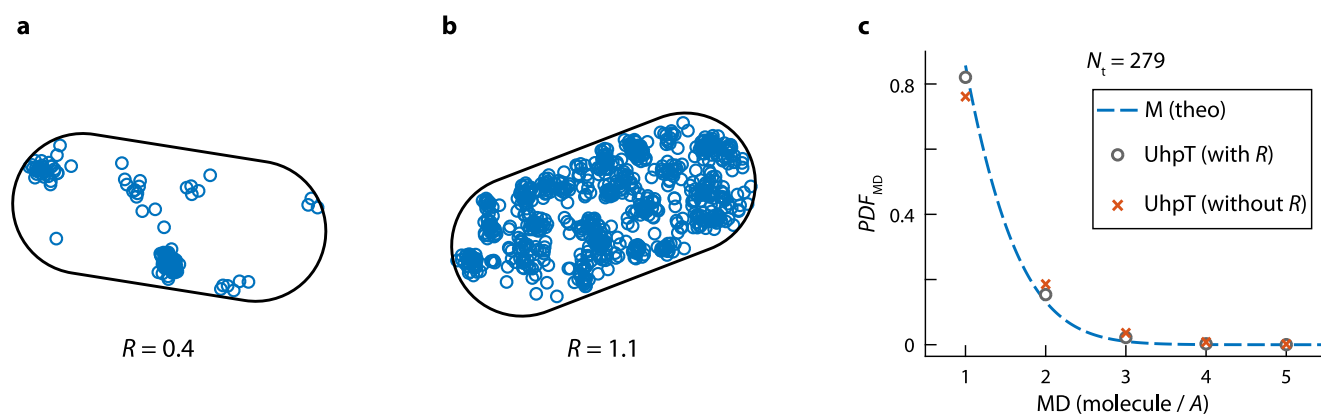


Figure 6. Application of randomness index R to remove complication of the cluster. (a,b) Examples of heterogeneous distribution of proteins in low (a) and high (b) molecule concentration conditions. (c) PDF_{MD} of UhpT with and without R -thresholding under low molecule concentration.

were determined by fitting the transmission images of each *E. coli* cell with a model of a cylinder capped by two hemispheres as described by Chen et al.¹⁹ The volume of the inner membrane is around 2–4% of the whole cell volume for bacteria based on the average size of typical *E. coli* cells (i.e., 2 μm long and 0.5 μm wide) as well as the average thickness of the outer membrane (4 nm), periplasmic space (11 nm), and inner membrane (4 nm).^{31,32} We estimated the $[M]_T$ by dividing the number of moles of protein by the volume of inner membrane. $[M]$ and $[D]$ were then calculated via multiplying $[M]_T$ with their corresponding populations. By calculating K_D under two molecule concentrations, we estimate that the K_D of SbmA in a cell is $490 \pm 366 \mu\text{M}$.

3.4. Ability of PDF_{MD} To Distinguish Membrane Proteins with Different Oligomeric States under High Molecule Concentrations. Figure 2b shows that the PDF_{MD} spreads and shifts to higher MD as molecule concentration increases. Such a spread resulting from high molecule concentration may raise the concern that PDF_{MD} cannot distinguish proteins with different oligomeric states at a high molecule concentration. To address this concern, we further examined the theoretical PDF_{MD} of monomeric to hexameric proteins at high molecule concentration. Figure 5a shows the same analysis as Figure 2a but with higher molecule number, $N_t = 4800$. Even though the difference between oligomeric states became smaller, the theoretical PDF_{MD} of each oligomeric state still shows its characteristic shape, indicating that PDF_{MD} can distinguish membrane proteins with different oligomeric states under high molecule concentrations.

As described in section 3.1, the PDF_{MD} can be well-fitted by a normalized truncated Gaussian function

$$G = \frac{1}{\sqrt{2\pi\sigma^2}} e^{-(x-\mu)^2/2\sigma^2}$$

where μ and σ are the mean and standard deviation of the distribution, respectively. To further explore how the molecule concentration and oligomeric state correlate with the truncated Gaussian function, we examined their effects on both μ and σ individually. Figure 5b,c shows the effect of molecule concentration using dimer, tetramer, and hexamer as examples. As the molecule concentration increases, the μ increases initially and decreases after $N_t > 600$. On the other hand, the σ monotonically increases with increasing molecule concentration for all oligomeric states. The hexamer also shows the most significant broadening (i.e., steepest slope) as molecule

concentration increases. Figure 5d,e shows the oligomeric-state-dependent μ and σ . In general, both μ and σ increase with oligomeric states, except when the oligomeric state = 1. Under the highest molecule concentration, the oligomeric-state dependence became weaker for μ but stronger for σ . Higher molecule concentration and oligomeric state both resulted in larger σ but had an opposite effect on μ . In terms of differentiating proteins with higher oligomeric states or higher molecule concentration, σ , could be a better parameter compared to PDF_{MD} and μ due to the larger difference at high molecule concentrations.

Note that our method quantifies the molecule concentration and PDF_{MD} simultaneously at the single-cell level. This allows comparison between cells with similar molecule concentration and naturally prevents confusion between the two cases: (1) lower oligomeric state with high molecule concentration and (2) higher oligomeric state with low molecule concentration.

3.5. Limitation of PDF_{MD} and Alternative Approaches.

Since our theoretical model is based on the assumption that proteins are randomly distributed on the membrane surface, PDF_{MD} is especially suitable to quantify the oligomeric states of proteins abundantly present on the cell surface (i.e., typically uniformly distributed). However, in the low molecule concentration condition, PDF_{MD} will be interfered with by the heterogeneous distribution of proteins. For example, heterogeneous distributions of proteins were both observed (Figure 6a,b, $R = 0.4$ and 1.1 for low and high concentration, respectively). In the low molecule concentration condition, the cluster resulted in large errors in estimating the PDF_{MD} and cannot report the correct oligomeric state. On the other hand, in the high molecule concentration condition, even though the clusters are still observable, the remaining localizations are sufficient to report the correct oligomeric states and alleviate the problem.

To determine the oligomeric states of proteins with low molecule concentration conditions by PDF_{MD} , cells with heterogeneous distribution need to be removed first. To do so, we first calculated the randomness index R for each *E. coli* cell (SI, Section 6) and its corresponding theoretical models.³³ The distribution of R for the theoretical models then provides the $R_{\text{threshold}}$ to remove the cells with proteins heterogeneously distributed on the membrane surface, thus leading to the final localizations for subsequent analysis. The application of R is only required when the number of localizations is low. Figure 6c shows the PDF_{MD} of UhpT with and without the R -

thresholding. The PDF_{MD} with the R -thresholding satisfactorily describes the theoretical model, suggesting the effectiveness of the R -thresholding approach to quantify the oligomeric states of membrane proteins under low molecule concentrations.

4. CONCLUSION

In conclusion, super-resolved localizations of membrane proteins allow direct assessment of their oligomeric states in cells, but the analysis can be complicated by the protein concentration, cell geometry, and photophysics of fluorescent tags. Here we develop a protein density function of molecule density (PDF_{MD}) approach to determine oligomeric states of abundant membrane proteins in cells. We first validated the PDF_{MD} approach with simulated single-molecule data and further applied it to investigate the oligomeric states of two membrane proteins, UhpT and SbmA. Our results suggest that UhpT exists as a monomer and SbmA exists as a mixture of monomer and dimer with an equilibrium dissociation constant of $\sim 490 \mu\text{M}$. The limitations, an alternative approach, and applicability of our method were also discussed. Our simulated results also suggest that this PDF_{MD} method is effective for membrane proteins with oligomeric states up to hexamer (Figure 2a–5a). Oligomeric-state-dependent PDF_{MD} of cytosolic proteins remains to be characterized with other techniques such as multicolor FRET.³⁴ Collectively, PDF_{MD} will allow us to directly access the function of proteins susceptible to its oligomeric state and may be applicable for other systems such as neuronal signal transduction.^{35,36}

■ ASSOCIATED CONTENT

Supporting Information

The Supporting Information is available free of charge on the ACS Publications website at DOI: 10.1021/acs.jpcc.8b10402.

Schematic overview of experimental strategy, construction of plasmids and strains, single-molecule imaging data simulation, photophysics of mEos3.2, and randomness index R (PDF)

■ AUTHOR INFORMATION

Corresponding Author

*E-mail: tchen37@central.uh.edu.

ORCID

Tai-Yen Chen: 0000-0002-2881-3068

Author Contributions

†X.X. and Y.-S.C. contributed equally.

Notes

The authors declare no competing financial interest.

■ ACKNOWLEDGMENTS

The authors gratefully acknowledge financial support from the University of Houston and the Welch Foundation (Grant NO. E-1947) and Prof. Peng Chen for the mEos3.2 plasmid.

■ REFERENCES

(1) Subburaj, Y.; Cosentino, K.; Axmann, M.; Pedrueza-Villalmanzo, E.; Hermann, E.; Bleicken, S.; Spatz, J.; García-Sáez, A. J. Bax Monomers Form Dimer Units in the Membrane That Further Self-Assemble into Multiple Oligomeric Species. *Nat. Commun.* **2015**, *6*, 8042.

(2) Mazurek, S.; Boschek, C. B.; Hugo, F.; Eigenbrodt, E. Pyruvate Kinase Type M2 and Its Role in Tumor Growth and Spreading. *Semin. Cancer Biol.* **2005**, *15* (4), 300–308.

(3) Guo, W.; Shi, L.; Javitch, J. A. The Fourth Transmembrane Segment Forms the Interface of the Dopamine D2 Receptor Homodimer. *J. Biol. Chem.* **2003**, *278* (7), 4385–4388.

(4) Fadoulglou, V. E.; Kokkinidis, M.; Glykos, N. M. Determination of Protein Oligomerization State: Two Approaches Based on Glutaraldehyde Crosslinking. *Anal. Biochem.* **2008**, *373* (2), 404–406.

(5) Loura, L. M. S.; Prieto, M. Fret in Membrane Biophysics: An Overview. *Front. Physiol.* **2011**, *2*, 82.

(6) Kaliszewski, M. J.; Shi, X.; Hou, Y.; Lingerak, R.; Kim, S.; Mallory, P.; Smith, A. W. Quantifying Membrane Protein Oligomerization with Fluorescence Cross-Correlation Spectroscopy. *Methods* **2018**, *140–141*, 40–51.

(7) Chen, Y.; Wei, L. N.; Müller, J. D. Probing Protein Oligomerization in Living Cells with Fluorescence Fluctuation Spectroscopy. *Proc. Natl. Acad. Sci. U. S. A.* **2003**, *100* (26), 15492–15497.

(8) Reznik, C.; Berg, R.; Foster, E.; Advincula, R.; Landes, C. F. Transient Three-Dimensional Orientation of Molecular Ions in an Ordered Polyelectrolyte Membrane. *J. Phys. Chem. Lett.* **2011**, *2* (6), 592–598.

(9) Chen, T.-Y.; Cheng, Y.-S.; Huang, P.-S.; Chen, P. Facilitated Unbinding Via Multivalency-Enabled Ternary Complexes: New Paradigm for Protein–DNA Interactions. *Acc. Chem. Res.* **2018**, *51* (4), 860–868.

(10) Sauer, M.; Heilemann, M. Single-Molecule Localization Microscopy in Eukaryotes. *Chem. Rev.* **2017**, *117* (11), 7478–7509.

(11) Liu, R.; Li, Y.; Liu, L. Single Molecule Fluorescence Spectroscopy for Quantitative Biological Applications. *Quant. Biol.* **2016**, *4* (3), 177–191.

(12) Chen, P.; Keller, A. M.; Joshi, C. P.; Martell, D. J.; Andoy, N. M.; Benítez, J. J.; Chen, T.-Y.; Santiago, A. G.; Yang, F. Single-Molecule Dynamics and Mechanisms of Metalloregulators and Metallochaperones. *Biochemistry* **2013**, *52* (41), 7170–7183.

(13) Durisic, N.; Laparra-Cuervo, L.; Sandoval-Alvarez, A.; Borbely, J. S.; Lakadamyali, M. Single-Molecule Evaluation of Fluorescent Protein Photoactivation Efficiency Using an in Vivo Nanotemplate. *Nat. Methods* **2014**, *11* (2), 156–162.

(14) Fricke, F.; Beaudouin, J.; Eils, R.; Heilemann, M. One, Two or Three? Probing the Stoichiometry of Membrane Proteins by Single-Molecule Localization Microscopy. *Sci. Rep.* **2015**, *5*, 14072.

(15) Ulbrich, M. H.; Isacoff, E. Y. Subunit Counting in Membrane-Bound Proteins. *Nat. Methods* **2007**, *4* (4), 319.

(16) Kasai, R. S.; Kusumi, A. Single-Molecule Imaging Revealed Dynamic GPCR Dimerization. *Curr. Opin. Cell Biol.* **2014**, *27*, 78–86.

(17) Veatch, S. L.; Machta, B. B.; Shelby, S. A.; Chiang, E. N.; Holowka, D. A.; Baird, B. A. Correlation Functions Quantify Super-Resolution Images and Estimate Apparent Clustering Due to over-Counting. *PLoS One* **2012**, *7* (2), e31457.

(18) Kasai, R. S.; Suzuki, K. G. N.; Prossnitz, E. R.; Koyama-Honda, I.; Nakada, C.; Fujiwara, T. K.; Kusumi, A. Full Characterization of GPCR Monomer–Dimer Dynamic Equilibrium by Single Molecule Imaging. *J. Cell Biol.* **2011**, *192* (3), 463–480.

(19) Chen, T.-Y.; Santiago, A. G.; Jung, W.; Krzemiński, Ł.; Yang, F.; Martell, D. J.; Helmann, J. D.; Chen, P. Concentration- and Chromosome-Organization-Dependent Regulator Unbinding from DNA for Transcription Regulation in Living Cells. *Nat. Commun.* **2015**, *6*, 7445.

(20) Gibb, B.; Ye, L. F.; Gergoudis, S. C.; Kwon, Y.; Niu, H.; Sung, P.; Greene, E. C. Concentration-Dependent Exchange of Replication Protein α on Single-Stranded DNA Revealed by Single-Molecule Imaging. *PLoS One* **2014**, *9* (2), e87922.

(21) Beshnova, D. A.; Cherstvy, A. G.; Vainshtein, Y.; Teif, V. B. Regulation of the Nucleosome Repeat Length in Vivo by the DNA Sequence, Protein Concentrations and Long-Range Interactions. *PLoS Comput. Biol.* **2014**, *10* (7), e1003698.

(22) Sing, C. E.; Olvera de la Cruz, M.; Marko, J. F. Multiple-Binding-Site Mechanism Explains Concentration-Dependent Unbinding Rates of DNA-Binding Proteins. *Nucleic Acids Res.* **2014**, *42* (6), 3783–3791.

(23) Chen, T.-Y.; Jung, W.; Santiago, A. G.; Yang, F.; Krzemiński, Ł.; Chen, P. Quantifying Multistate Cytoplasmic Molecular Diffusion in Bacterial Cells Via Inverse Transform of Confined Displacement Distribution. *J. Phys. Chem. B* **2015**, *119* (45), 14451–14459.

(24) Javer, A.; Long, Z.; Nugent, E.; Grisi, M.; Siriwatwetchakul, K.; Dorfman, K. D.; Cicuta, P.; Cosentino Lagomarsino, M. Short-Time Movement of E. Coli Chromosomal Loci Depends on Coordinate and Subcellular Localization. *Nat. Commun.* **2013**, *4*, 3003.

(25) Annibale, P.; Scarselli, M.; Greco, M.; Radenovic, A. Identification of the Factors Affecting Co-Localization Precision for Quantitative Multicolor Localization Microscopy. *Opt. Nanoscopy* **2012**, *1* (1), 9.

(26) Frost, N. A.; Lu, H. E.; Blanpied, T. A. Optimization of Cell Morphology Measurement Via Single-Molecule Tracking Palm. *PLoS One* **2012**, *7* (5), e36751.

(27) Lee, S.-H.; Shin, J. Y.; Lee, A.; Bustamante, C. Counting Single Photoactivatable Fluorescent Molecules by Photoactivated Localization Microscopy (Palm). *Proc. Natl. Acad. Sci. U. S. A.* **2012**, *109* (43), 17436–17441.

(28) Ambudkar, S. V.; Anantharam, V.; Maloney, P. C. Uhpt, the Sugar Phosphate Antiporter of Escherichia Coli, Functions as a Monomer. *J. Biol. Chem.* **1990**, *265* (21), 12287–12292.

(29) Runti, G.; Lopez Ruiz, M. d. C.; Stoilova, T.; Hussain, R.; Jennions, M.; Choudhury, H. G.; Benincasa, M.; Gennaro, R.; Beis, K.; Scocchi, M. Functional Characterization of Sbma, a Bacterial Inner Membrane Transporter Required for Importing the Antimicrobial Peptide Bac7(1–35). *J. Bacteriol.* **2013**, *195* (23), 5343–5351.

(30) Corbalan, N.; Runti, G.; Adler, C.; Covaceuszach, S.; Ford, R. C.; Lamba, D.; Beis, K.; Scocchi, M.; Vincent, P. A. Functional and Structural Study of the Dimeric Inner Membrane Protein Sbma. *J. Bacteriol.* **2013**, *195* (23), 5352–5361.

(31) Graham, L.; Beveridge, T.; Nanninga, N. Periplasmic Space and the Concept of the Periplasm. *Trends Biochem. Sci.* **1991**, *16*, 328–329.

(32) Mitra, K.; Ubarretxena-Belandia, I.; Taguchi, T.; Warren, G.; Engelman, D. M. Modulation of the Bilayer Thickness of Exocytic Pathway Membranes by Membrane Proteins Rather Than Cholesterol. *Proc. Natl. Acad. Sci. U. S. A.* **2004**, *101* (12), 4083–4088.

(33) Dry, M. J.; Preiss, K.; Wagemans, J. Clustering, Randomness and Regularity: Spatial Distributions and Human Performance on the Traveling Salesperson Problem and Minimum Spanning Tree Problem. *The Journal of Problem Solving* **2012**, *4* (1), 2.

(34) Keller, A. M.; DeVore, M. S.; Stich, D. G.; Vu, D. M.; Causgrove, T.; Werner, J. H. Multicolor Three-Dimensional Tracking for Single-Molecule Fluorescence Resonance Energy Transfer Measurements. *Anal. Chem.* **2018**, *90* (10), 6109–6115.

(35) Proctor, E. A.; Fee, L.; Tao, Y.; Redler, R. L.; Fay, J. M.; Zhang, Y.; Lv, Z.; Mercer, I. P.; Deshmukh, M.; Lyubchenko, Y. L.; et al. Nonnative Sod1 Trimer Is Toxic to Motor Neurons in a Model of Amyotrophic Lateral Sclerosis. *Proc. Natl. Acad. Sci. U. S. A.* **2016**, *113* (3), 614–619.

(36) Patrizio, A.; Specht, C. G. Counting Numbers of Synaptic Proteins: Absolute Quantification and Single Molecule Imaging Techniques. *Neurophotonics* **2016**, *3* (4), 041805–041805.